

# Induced four fold anisotropy and bias in compensated NiFe/FeMn double layers

T. Mewes

*Department of Physics, 1077 Smith Laboratory  
Ohio State University  
174 W 18th Ave, Columbus, OH 43210, USA*

B. Hillebrands

*Fachbereich Physik  
Universität Kaiserslautern  
Erwin Schrödinger Str. 56,  
67663 Kaiserslautern, Germany*

R. L. Stamps\*

*School of Physics, M013  
University of Western Australia  
35 Stirling Highway, Crawley, WA 6009, Australia*

(Dated: October 31, 2018)

A vector spin model is used to show how frustrations within a multisublattice antiferromagnet such as FeMn can lead to four-fold magnetic anisotropies acting on an exchange coupled ferromagnetic film. Possibilities for the existence of exchange bias are examined and shown to exist for the case of weak chemical disorder at the interface in an otherwise perfect structure. A sensitive dependence on interlayer exchange is found for anisotropies acting on the ferromagnet through the exchange coupling, and we show that a wide range of anisotropies can appear even for a perfect crystalline structure with an ideally flat interface.

## I. INTRODUCTION

It is interesting to note that some of the technologically most important exchange bias systems are also some of the most complex and difficult to understand. Antiferromagnetic metal compounds, such as FeMn, can be used to pin ferromagnetic layers, making them attractive for application in some devices. The unidirectional and higher order magnetic anisotropies that appear in bilayers containing FeMn seem to vary widely between experiments, and there is no model yet capable of explaining the underlying microscopic mechanisms.

One particularly intriguing unanswered question is how exchange bias can occur in structures with compensated interfaces. Being compensated, the ferromagnet spins in such structures interact equally strongly with spins from all antiferromagnetic sublattices. In the simplest approximation, there is no net magnetic moment in the antiferromagnet for the ferromagnet to couple to, and hence no way for the antiferromagnet to bias a magnetization loop. A closer examination reveals that the antiferromagnetic order at the interface is likely to be frustrated, and a new configuration resulting in a small magnetic moment at the interface should form<sup>1</sup>. However it has been shown that this so-called 'spin-flop' coupling is not of its own accord able to support exchange bias during a magnetization loop measurement<sup>2,3</sup>.

A number of considerations have been discussed that may explain the existence of exchange bias in compen-

sated interface structures. It is highly likely that the interfaces are not perfectly compensated due to defects in structure and chemical composition. These imperfections of the interface give rise to small numbers of uncompensated spins that can result in weak bias shifts.

A second unanswered question is why the magnitude of the bias shift is much smaller than the exchange field coupling the ferromagnet and antiferromagnet. A number of possible explanations have been put forward. These include the formation and pinning of a partial domain wall near the interface<sup>4</sup>, the pinning of domains and domain walls in the antiferromagnet<sup>5,6,7</sup>, and interactions between grains in thin antiferromagnetic films<sup>8</sup>. In each explanation there are either restrictions on film thickness or reliance on the existence of structural or chemical disorder that make comparison to experiment difficult.

As most models proposed so far focussed on explaining the magnitude of the bias shift, they do not account for the drastically increased coercivity observed in exchange bias systems. While spin-flop coupling is not able to shift the magnetization loop it does give rise to increased coercivity in systems with a two sublattice antiferromagnet by inducing a two-fold anisotropy in the ferromagnet<sup>3</sup>.

In the present paper we demonstrate how frustrations within a multisublattice antiferromagnet such as FeMn can lead to four-fold magnetic anisotropies acting on the ferromagnet. As has been shown previously the interplay between unidirectional and induced higher order anisotropies acting on the ferromagnet not only causes

an increased coercivity but can also account for some of the complex dependencies on applied field angle observed in exchange bias systems<sup>9,10,11,12,13,14,15</sup>.

The possibility of exchange bias for a multisublattice antiferromagnet is examined and shown for the case of weak chemical disorder at the interface in an otherwise perfect structure. Most importantly, we identify a sensitive dependence for the anisotropies on interlayer exchange, and show that a wide range of induced anisotropies can appear even for a perfect crystalline structure with an ideally flat interface.

The paper is organized as follows. A vector spin model for FeMn is introduced in the next section, followed by results obtained in the limit of large interlayer exchange coupling. Interesting possibilities for multiple configurations and effective anisotropies appear with small interlayer coupling, and are discussed in section III. The possibility of exchange bias in a perfectly compensated system is discussed in section IV.

## II. VECTOR SPIN MODEL AND BULK EQUILIBRIUM SPIN STATES

Magnetic order in metallic antiferromagnets such as Fe<sub>50</sub>Mn<sub>50</sub> is very difficult to predict from first principles. One particularly difficult aspect of the problem is the importance of contributions that appear as magnetic anisotropies that are ultimately determined by spin orbit coupling effects inside a crystalline geometry. The problem of determining spin configurations associated with exchange bias further requires consideration of a large number of atoms in both the ferromagnet and antiferromagnet films. These considerations make the problem very difficult to approach from a quantum mechanical point of view.

In view of these difficulties, phenomenological approaches are useful for developing insights into the problem. In this work we represent the spin configuration using vector spins arranged at lattice sites that represent the atomic ordering of a Ni<sub>81</sub>Fe<sub>19</sub>/Fe<sub>50</sub>Mn<sub>50</sub> two film exchange coupled crystalline structure. Equilibrium spin configurations are found as steady state solutions to coupled sets of classical torque equations for each spin  $\mathbf{S}_i$  located at site  $i$ :

$$\frac{d}{dt}\mathbf{S}_i = \gamma\mathbf{S}_i \times \frac{\partial\mathcal{H}}{\partial\mathbf{S}_i} + \alpha\mathbf{S}_i \times \mathbf{S}_i \times \frac{\partial\mathcal{H}}{\partial\mathbf{S}_i}. \quad (2.1)$$

The first term in this equation represents free precession of spin  $\mathbf{S}_i$  in its local field calculated from an appropriate Hamiltonian,  $\mathcal{H}$ . The second term is dissipative with a form chosen to preserve the length of the spin vector. The calculation is intended to find equilibria only, and so the parameters  $\gamma$  and  $\alpha$  are used only to control stability and convergence so that the resulting dynamics does not represent specific physical processes.

The Hamiltonian is chosen to be in the form of a Heisenberg spin array with exchange interactions  $J_{i,j}$ , a

Zeeman term for an external applied field  $\mathbf{H}$ , and four-fold anisotropies  $K_i^{(1)}$  and  $K_i^{(2)}$ . The exact form used is

$$\begin{aligned} \mathcal{H} = \sum_i & \left[ -g\mu_B\mathbf{H} \cdot \mathbf{S}_i - 2 \sum_{\delta} J_{i,i+\delta} \mathbf{S}_i \cdot \mathbf{S}_{i+\delta} \right. \\ & + K_i^{(1)} (S_{i,x}^2 S_{i,y}^2 + S_{i,x}^2 S_{i,z}^2 + S_{i,z}^2 S_{i,y}^2) \\ & \left. + K_i^{(2)} S_{i,x}^2 S_{i,y}^2 S_{i,z}^2 \right]. \end{aligned} \quad (2.2)$$

The exchange sum is over nearest neighbors at sites  $i+\delta$ , and the constants  $g$  and  $\mu_B$  are the Landé factor and Bohr Magneton, respectively. Units are such that Eq. 2.2 is an energy density.

All calculations reported here assume fcc lattice structure for both ferromagnet and antiferromagnet. The anisotropy of the antiferromagnet is chosen to mimic the 3Q phase of an fcc antiferromagnet. It is useful to note that there are three simple stable equilibrium configurations, and it is not entirely clear from experiment which is favored in Fe<sub>50</sub>Mn<sub>50</sub><sup>16,17,18,19</sup>. Recent calculations suggest the 3Q phase to be the stable low energy configuration of bulk Fe<sub>50</sub>Mn<sub>50</sub><sup>20,21</sup>. The 3Q phase is realised in the vector spin model if the anisotropies fulfill both of the conditions  $K_i^{(1)}/K_i^{(2)} < -1/9$  and  $K_i^{(1)}/K_i^{(2)} < -4/9$ . This phase has spins aligned along cube diagonals as illustrated in Fig. 1 (a). All calculations were made using periodic boundary conditions in all directions.

The spin structure calculated using the above model for Fe<sub>50</sub>Mn<sub>50</sub> is strongly affected by surfaces in a thin film geometry, due to the broken translational symmetry at the interfaces. This especially is true when the antiferromagnetic film is exchange coupled to a ferromagnet. An example is shown in Fig. 1 (b) where two atomic layers of ferromagnetically coupled spins are exchange coupled to an Fe<sub>50</sub>Mn<sub>50</sub> film. Antiferromagnetic anisotropies are  $K_i^{(1)} = -|J_{AF}|/10$ , and  $K_i^{(2)} = |J_{AF}|/10$  where  $J_{AF}$  is the exchange coupling in the antiferromagnet. No anisotropy is assumed in the ferromagnet in order to mimic properties of Ni<sub>81</sub>Fe<sub>19</sub>. The ratio of ferromagnet to antiferromagnet exchange energies is set at  $J_F/|J_{AF}| = 1.55$ . These values represent exchange energies consistent with the ratio of ordering temperatures of Ni<sub>81</sub>Fe<sub>19</sub> and Fe<sub>50</sub>Mn<sub>50</sub>.

The calculation of a spin configuration is performed in analogy to a field cooling procedure. The ferromagnet spins are aligned parallel in plane at an angle  $\alpha_M$  made with respect to the (001) direction. The antiferromagnet spins are initially oriented randomly. The equations of motion are integrated numerically until the condition

$$\sum_i \frac{1}{|\mathbf{S}_i|} \left| \frac{d\mathbf{S}_i}{dt} \Delta t \right| < \epsilon \quad (2.3)$$

is satisfied where  $\epsilon$  is taken to be on the order of  $10^{-9}$ .

An interesting feature of the spin configuration shown in Fig. 1(b) is the near complete antiparallel alignment

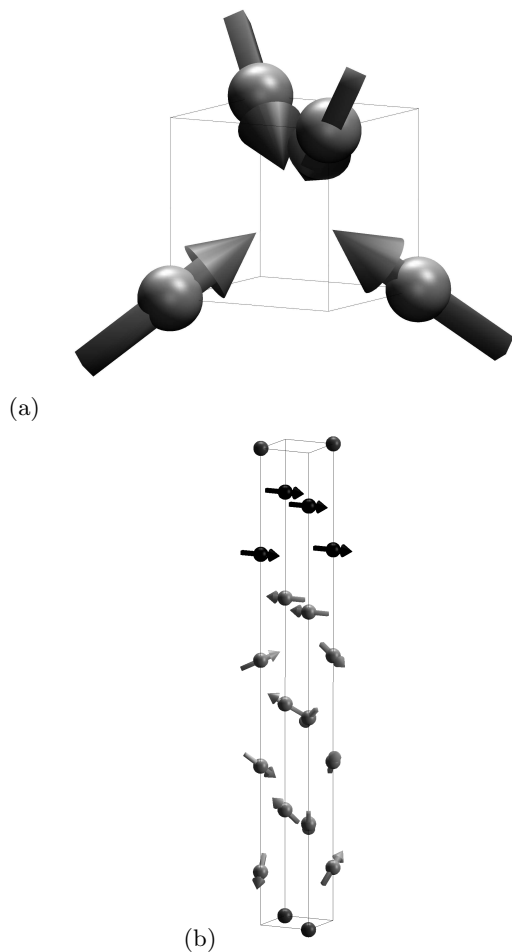


FIG. 1: The  $3Q$  phase for bulk  $\text{Fe}_{50}\text{Mn}_{50}$  are shown in (a). An example configuration of spins is shown in (b) for  $\text{Fe}_{50}\text{Mn}_{50}$  exchange coupled to two layers of  $\text{Ni}_{81}\text{Fe}_{19}$ . The dark spheres indicate locations within  $\text{Ni}_{81}\text{Fe}_{19}$ . Periodic boundary conditions are assumed in all directions in (a), and in directions parallel to the film planes in (b).

of spins directly at the interface due to the strong coupling between the ferromagnet and the antiferromagnet assumed in this case. This leads to a strong modification of the entire spin structure of the antiferromagnet to the extent that it no longer resembles the  $3Q$  structure. The ordering at and near the interface is sensitive to the magnitude of the interlayer exchange coupling  $J_{F,AF}$ , and a number of different configurations with similar energies are possible. It will be shown below that this has consequences on the effective anisotropies acting on the ferromagnet, and also on possible mechanisms for exchange bias.

### III. INDUCED ANISOTROPY AND COERCIVITY

The magnetic anisotropies in the antiferromagnet are communicated to the ferromagnet through the interac-

tion at their common interface. Cases of strong exchange coupling across the interface and weak exchange coupling show strikingly different features because of how spins order in the antiferromagnet.

#### A. Strong interlayer coupling

The strong interlayer exchange responsible for the antiparallel ordering of spins near the interface in Fig. 1(b) provides a mechanism for anisotropies to be induced in the ferromagnet. If the orientation of the ferromagnet is changed through application of an external applied field, spins in the antiferromagnet will be rotated through anisotropy easy and hard axes. This affects the total energy of the system, and in particular can be represented by effective fields acting on the ferromagnet. The energy per spin is defined for  $N_F$  ferromagnet spins and  $N_{AF}$  antiferromagnet spins in a unit cell of the two film structure as

$$\varepsilon_{F,AF} = \frac{E_{F,AF}}{N_F + N_{AF}}, \quad (3.1)$$

where  $E_{F,AF}$  is the total energy of the two film system. The energy density  $\varepsilon_{F,AF}$  for an  $N_F = 4$  and  $N_{AF} = 12$  system, as depicted in Fig. 1, is shown in Fig. 2(a). The energy is shown as a function of angle  $\alpha_M$  and is calculated by fixing the orientation of the ferromagnet spins and allowing the antiferromagnet spins to relax using the field cooling procedure described earlier. The field cooling process was repeated for each orientation value of  $\alpha_M$ . The results of this procedure were compared to results from an alternate method by which the antiferromagnet was field cooled along  $\alpha_M = 0$  and the energy calculated for each new  $\alpha_M$  without additional field cooling. The two different calculation procedures produced identical results.

It is clear from Fig. 2(a) that interlayer coupling between the ferromagnet and antiferromagnet results in a total energy for the system with four-fold symmetry for the in-plane orientation of the ferromagnet. The solid line in Fig. 2 is a fit using

$$\varepsilon_{F,AF} = K_4^{eff} \sin^2(\alpha_M - \alpha_4) \cos^2(\alpha_M - \alpha_4) \quad (3.2)$$

where  $\alpha_4$  describes the orientation of the anisotropy easy and hard axes with respect to the [100] crystallographic direction.

Magnetization loops calculated for this set of  $K_i^{(1)}$ ,  $K_i^{(2)}$ , and  $J_{F,AF}$  parameters show properties consistent with a simple four fold anisotropy of the form in Eq. 3.2. An example is shown in Fig. 2(b) for a field applied along the [110] and [100] directions. The magnetization is given in units of Bohr Magneton and is defined as  $\mu_S = -g\mu_B \sum_i^{N_F} |\mathbf{S}_i|$ . The easy direction is for  $\alpha_4 = \pi/4$ . There is coercivity for the field along the easy

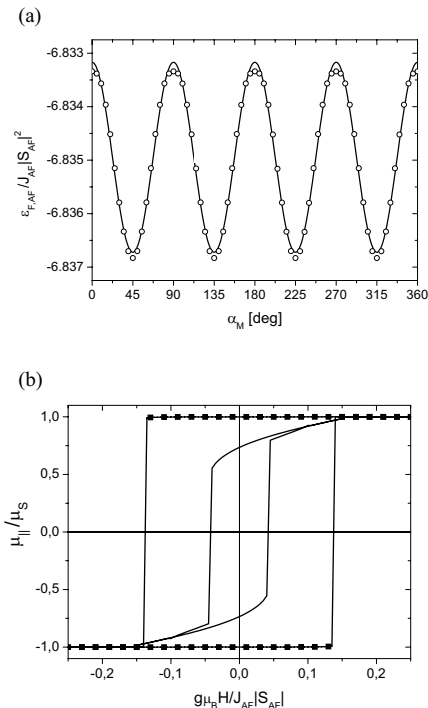


FIG. 2: Total energy per spin is shown in (a) as a function of ferromagnet orientation. The angle  $\alpha_M$  is measured with respect to the  $[100]$  axis. The effective anisotropy displayed by the ferromagnet is four fold, without a bias shift. An example magnetization loop is shown in (b) for the applied field along the  $[110]$  (filled circles) and  $[100]$  (solid line) directions.

direction as would be expected due to the existence of stable and metastable states for the ferromagnet parallel and antiparallel to the applied field. Coercivity along the hard direction exists because of the zero field remanent magnetization aligned along an easy direction.

### B. Moderate and weak interlayer coupling

In the case of large  $J_{F,AF}$  the magnetic behaviour of the ferromagnet is dominated by the intra- and interlayer exchange coupling and is well described by a simple four fold anisotropy. When  $J_{F,AF}$  is not large relative to  $J_{AF}$ , new possibilities for metastable ordering within the antiferromagnet appear. Examination of results from numerical solutions to Eq. 2.1 reveal multiple equilibrium configurations with comparable but different energies. An example of this behavior is shown in Fig. 3 where the total energy  $\varepsilon_{F,AF}$  is shown as a function of angle for an interlayer exchange coupling  $J_{F,AF} = -0.3|J_{AF}|$ . The parameters and geometry are otherwise as used for the example shown in Fig. 2. These results were generated using the field cooling procedure at each angle. At each angle, thirty different random initial configurations for the antiferromagnet spins were used, resulting in a spread of energies as shown in Fig. 3(a). The range of

energies at each angle represents a sampling of different possible spin configurations.

The open symbols connected by the thick solid line in Fig. 3(a) are the lowest energies found during the cooling process. In Fig. 3(b) the lowest energies are plotted separately to more clearly show the four-fold symmetry of the ground state energies. Note that the energy  $\varepsilon_{F,AF}$  displays very sharp maxima and is only approximately consistent with the  $K_4^{eff}$  as given in Eq. 3.2.

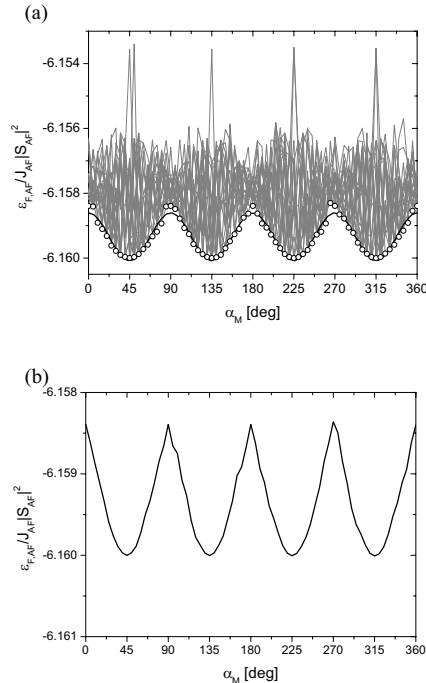


FIG. 3: Total energy as a function of angle with  $J_{F,AF} = -0.5|J_{AF}|$ . Other parameters and structure are the same as used for Fig. 2. In (a), energies from thirty different random initial configurations calculated at each angle are shown. The spread in energies at each angle is due to the existence of several metastable spin configurations within the antiferromagnet. The lowest energies found are identified by open symbols in (a) and plotted together in (b).

The degree to which the lowest energy configurations result in an anisotropy approximating that described by Eq. 3.2 is strongly dependent on the strength of the interlayer coupling  $J_{F,AF}$ . For some values of  $J_{F,AF}$ , even the sign of the effective anisotropy can change, representing a change in the orientation of the easy and hard axes. The magnitude and sign of  $K_4^{eff}$  saturates to a fixed value for  $J_{F,AF}$  larger than  $1.25|J_{AF}|$ . At these large values, the antiferromagnet spins at the interface are aligned collinear with respect to the ferromagnet spins, and rotate rigidly with the ferromagnet as described in the previous chapter.

A plot of the effective anisotropy determined by fitting the ground state energy configurations to Eq. 3.2 is given in Fig. 4 as a function of interlayer coupling

$J_{F,AF}$ . The goodness of fit is quantified by the measure  $R^2$  where  $R^2 = 1$  is very good and denoted by lightly shaded stripes, and very bad bits are denoted by dark gray stripes.

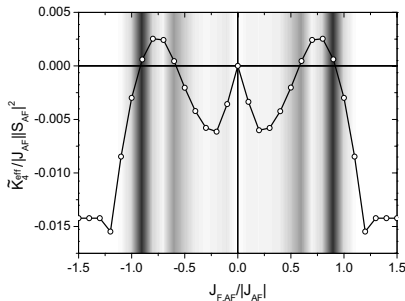


FIG. 4: Effective anisotropy describing ground state energy configurations as a function of interlayer coupling  $J_{F,AF}$ . The degree to which the anisotropy is a simple four-fold type of the form given in Eq. 3.2 is indicated by grayscale shading. White means that the description is very good, and black means that the description is very poor. Note that the direction of the easy and hard axes can change depending on the magnitude of  $J_{F,AF}$ .

It is interesting to examine separately the ferromagnet and antiferromagnet contributions to  $\varepsilon_{F,AF}$ . In particular, the ferromagnet component of the energy can have a different dependence on orientation angle  $\alpha_M$  than the total system energy. A way of thinking of this is to consider the effective field  $\mathbf{h}_{eff}$  acting at a layer of spins within the structure and calculate the associated energy  $-\mathbf{S}_i \cdot \mathbf{h}_{eff}$ . The field varies in magnitude and direction throughout the structure, and can have a dependence on  $\alpha_M$  that also varies from layer to layer. A way of characterizing this difference in a meaningful way is to identify extrema in the energy of the ferromagnet calculated as a function of  $\alpha_M$ , and compare this to the extrema determined from the total energy  $\varepsilon_{F,AF}$ .

Results of this characterization are given in Fig. 5 as the angles  $\alpha_M$  where minima (a) and maxima (b) occur as functions of  $J_{F,AF}$ . The angles  $\alpha_{min,F}$  represent orientations of the ferromagnet spins where the energy of the ferromagnet spins has minima, and the angles  $\alpha_{min,F+AF}$  represent orientations of the ferromagnet spins where the energy of the entire system has minima. Likewise, the angles  $\alpha_{max,F}$  represent orientations of the ferromagnet spins where the energy of the ferromagnet spins has maxima, and the angles  $\alpha_{max,F+AF}$  represent orientations of the ferromagnet spins where the energy of the entire system has maxima.

An interpretation of the minima is to assign different easy and hard axes to the ferromagnet and system. In this view, the alignment of the ferromagnet to an easy axis associated with the system rather than the easy axis defined by the local effective field acting on the ferromagnet is a clear indication of how order in the antiferromag-

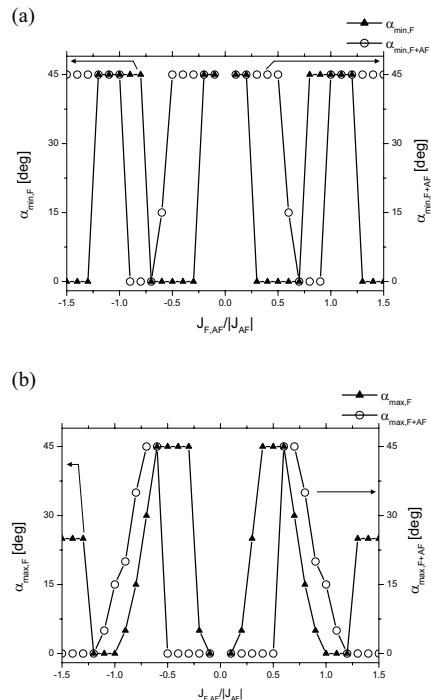


FIG. 5: Orientations for energy extrema as functions of  $J_{F,AF}$ . In (a), angles  $\alpha_{min,F}$  represent orientations of the ferromagnet spins where the energy of the ferromagnet spins has minima, and the angles  $\alpha_{min,F+AF}$  represent orientations of the ferromagnet spins where the energy of the entire system has minima. In (b) the angles  $\alpha_{max,F}$  and  $\alpha_{max,F+AF}$  are shown for the corresponding energy maxima.

net is involved in determining the magnetic anisotropies observable through the ferromagnet. As an extreme example, the large  $J_{F,AF}$  limit shown in Fig. 5 has the ferromagnet 'easy' axis parallel to the system hard axis. This occurs again at smaller values of  $J_{F,AF}$ .

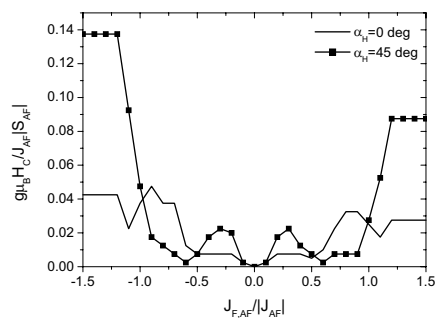


FIG. 6: Coercive fields for applied fields along the [110] and [100] directions for different interlayer couplings  $J_{F,AF}$ . The closed symbols are for the applied field directed along the [110] and the open symbols are for the applied field directed along [100].

Coercivities calculated for magnetization loop simula-

tions also show curious behavior for some values of interlayer coupling. Coercive fields for applied fields along the [110] and [100] directions are shown in Fig. 6. The most curious feature is the different coercivities produced with positive and negative  $J_{F,AF}$ . The reason for this is that the antiferromagnetic film used for the calculation is very thin. Large values of  $|J_{F,AF}|$  fully align the spins colinear with the ferromagnet and contribute to the net magnetic moment. When  $J_{F,AF} > 0$ , the contribution increases the Zeeman energy of the system in an applied field, and when  $J_{F,AF} < 0$ , the contribution decreases the Zeeman energy in an applied field. The easy axis coercivities are therefore larger with negative  $J_{F,AF}$  than with positive  $J_{F,AF}$ .

#### IV. MECHANISMS FOR EXCHANGE BIAS

The anisotropies induced on the ferromagnet through interlayer exchange coupling with the ferromagnet were not found to contain any unidirectional contribution in any of the compensated interface examples studied. This is consistent with previous calculations demonstrating the inability of spin flop coupling at compensated interfaces to support exchange bias shifts using physically reasonable assumptions for anisotropy fields<sup>3,22</sup>.

##### A. Bias with interface defect

It has been noted that small regions of uncompensated spins at the interface can be sufficient to create exchange bias<sup>3,7,23,24</sup>. This possible mechanism for exchange bias is explored for the  $\text{Ni}_{81}\text{Fe}_{19}/\text{Fe}_{50}\text{Mn}_{50}$  model discussed here. The unit cell of the structure with defect is based on eight antiferromagnet atomic layers with eight spins in each layer exchange coupled to a ferromagnet film consisting of two atomic layers, also with eight spins per layer. Periodic boundary conditions in the planes parallel to the interface as used. The defect is represented by replacing the exchange couplings and local anisotropies of one spin on the ferromagnet side of the interface with values appropriate to the antiferromagnet. In this way the unit cell of the structure has 15 ferromagnetically coupled spins, and 65 antiferromagnetically coupled spins, with a small uncompensated region at the interface.

Results from calculations for coupling between ferromagnet and antiferromagnet spins with  $J_{F,AF} = -0.5|J_{AF}|$  are shown in Fig. 7. A small negative bias of magnitude  $0.005|J_{AF} S_{AF}|/(g\mu_B)$  appears. It is interesting to note that a simple estimate of the shift would be to average the uncompensated coupling energy  $2J_{F,AF}$  over the number of ferromagnet spins, giving a bias field of  $0.07|J_{AF} S_{AF}|/(g\mu_B)$ . The factor of fourteen discrepancy is because the spin order in the antiferromagnet changes during magnetization in such a way as to reduce the magnitude of the field necessary to align the ferromagnet. This is analogous to the reduction in bias field

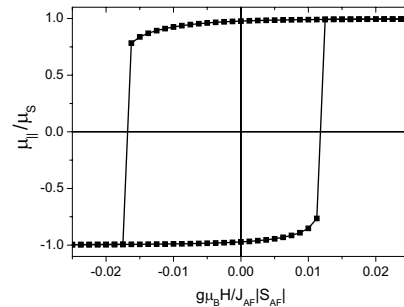


FIG. 7: Biased magnetization loop with one defect spin. The parameters used are the same as those used for the unbiased loop shown in Fig. 2(b). The difference is that here the unit cell has  $N_F = 15$ ,  $N_{AF} = 65$ , and one spin 'defect' located at the interface providing a small net uncompensated antiferromagnetic moment.  $J_{F,AF}$  is  $-0.5|J_{AF}|$ .

described by Mauri, et al<sup>4</sup> for exchange bias with completely uncompensated interfaces.

#### V. SUMMARY

A molecular field model of magnetic order in multi-sublattice magnets, such as  $\text{Fe}_{50}\text{Mn}_{50}$ , exchange coupled to a ferromagnet has been examined. It has been shown that ordering of spins near the surfaces and interfaces of the antiferromagnet are strongly affected by exchange coupling, but that the intrinsic four-fold anisotropy of the antiferromagnet is still induced into the ferromagnet. Through exchange coupling, the ferromagnet spins experience a four-fold anisotropy with a magnitude sensitive to the strength of the interlayer coupling. An important point is that the nature of the anisotropy is also dependent on the strength of the coupling, and is only strictly of a simple four fold form in the case of strong interlayer coupling.

Weak and moderate values of interlayer coupling lead to an additional interesting effect on the induced anisotropy. Rather than a single well defined order in the antiferromagnet, a number of metastable configurations appear. The lowest energy configurations lead to an induced anisotropy with four-fold symmetry. The degree to which the four-fold anisotropy associated with the lowest energy configurations is described by a simple sinusoid depends on the strength of the interlayer exchange coupling and is only approximate at best for some values of the exchange.

Exchange bias shifts for perfectly compensated interfaces assuming the low energy spin configuration was not found. Instead, an exchange bias could be created by allowing the interface to have some small degree of uncompensation through introduction of a defect in the interface structure. These findings are consistent with previous work showing that a spin-flop configuration at a

compensated interface is incapable of producing a shifted magnetization loop, whereas mixed interfaces with some amount of uncompensation present can shift the magnetization loop.

### Acknowledgments

TM and RLS acknowledge support by the Australian Research Council (Discovery Grant and IREX).

- 
- \* Electronic address: stamps@physics.uwa.edu.au
- <sup>1</sup> N. C. Koon, Phys. Rev. Lett. **78**, 4865-4868 (1997).
  - <sup>2</sup> T. C. Schulthess, W. H. Butler, Phys. Rev. Lett. **81**, 4516-4519 (1998).
  - <sup>3</sup> T. C. Schulthess, W. H. Butler, J. Appl. Phys. **85**, 5510-5515 (1999).
  - <sup>4</sup> D. Mauri, H. C. Siegmann, P. S. Bagus, E. Kay, J. Appl. Phys. **62**, 3047-3049 (1987).
  - <sup>5</sup> A. P. Malozemoff, Phys. Rev. B **37**, 7673-7679 (1988).
  - <sup>6</sup> P. Miltényi, M. Gierlings, J. Keller, B. Beschoten, G. Güntherodt, U. Nowak, K. D. Usadel, Phys. Rev. Lett. **84**, 4224-4227 (2000).
  - <sup>7</sup> U. Nowak, A. Misra, K. D. Usadel, J. Appl. Phys. **89**, 7269-7271 (2001).
  - <sup>8</sup> D. Suess, M. Kirschner, T. Schrefl, W. Scholz, R. Dittrich, H. Forster, J. Fidler, J. Appl. Phys. **93**, 8618-8620 (2003).
  - <sup>9</sup> Haiwen Xi, Robert M. White, J. Appl. Phys. **86**, 5169-5174 (1999).
  - <sup>10</sup> H. J. Santos, F. A. Pinheiro, A. Y. Takeuchi, L. C. Sampaio, R. A. Simão, C. A. Achete, M. Cremona, Phys. Rev. B **60**, 6871 (1999).
  - <sup>11</sup> T. Pokhil, E. Linville, S. Mao, J. Appl. Phys. **89**, 6588-6590 (2001).
  - <sup>12</sup> Chih-Huang Lai, Yung-Hung Wang, Ching-Ray Chang, Jyh-Shinn Yang, Y. D. Yao, Phys. Rev. B **64**, 094420 (2001)
  - <sup>13</sup> Y. J. Tang, B. F. P. Roos, T. Mewes, A. R. Frank, M. Rickart, M. Bauer, S. O. Demokritov, B. Hillebrands, X. Zhou, B. Q. Liang, X. Chen, W. S. Zhan, Phys. Rev. B **62**, 8654-8657 (2000).
  - <sup>14</sup> T. Mewes, H. Nembach, M. Rickart, S. O. Demokritov, J. Fassbender, B. Hillebrands, Phys. Rev. B **65**, 224423 (2002).
  - <sup>15</sup> M. J. Pechan, D. Bennett, N. Teng, C. Leighton, J. Nogués, I. K. Schuller, Phys. Rev. B **65**, 064410 (2002).
  - <sup>16</sup> J.S. Kouvel, J.S. Kasper, J. Phys. Chem. Solids **24**, 529 (1963).
  - <sup>17</sup> H. Umebayashi, Y. Ishikawa, J. Phys. Soc. Japan **21**, 1281 (1966).
  - <sup>18</sup> S.J. Kennedy, T.J. Hicks, J. Phys. F **17**, 1599 (1987).
  - <sup>19</sup> T.C. Schulthess, W.H. Butler, G.M. Stocks, S. Maat, G.J. Mankey, J. Appl. Phys. **85**, 4842 (1999).
  - <sup>20</sup> J.M. MacLaren, S. Crampin, D.D. Vvedensky, J.B. Pendry, Phys. Rev. B **40**, 12164 (1989).
  - <sup>21</sup> J.M. MacLaren, S. Crampin, D.D. Vvedensky, Phys. Rev. B **40**, 12176 (1989).
  - <sup>22</sup> M. D. Stiles, R. D. McMichael, Phys. Rev. B **63**, 064405 (2001).
  - <sup>23</sup> J. S. Kouvel, J. Phys. Chem. Solids **24**, 795-822 (1963).
  - <sup>24</sup> R. E. Camley, B. V. McGrath, R. J. Astalos, R. L. Stamps, Joo-Von Kim, L. Wee, J. Vac. Sci. Technol. A **17**, 1335-1339 (1999).